Crystal Growth Hot Paper

Deutsche Ausgabe: DOI: 10.1002/ange.201511792
Internationale Ausgabe: DOI: 10.1002/anie.201511792

Formation of Hybrid Perovskite Tin Iodide Single Crystals by Top-Seeded Solution Growth

*Yangyang Dang, Yian Zhou, Xiaolong Liu, Dianxing Ju, Shengqing Xia, Haibing Xia, and Xutang Tao**

Abstract: *Hybrid perovskites have generated a great deal of interest because of their potential in photovoltaic applications. However, the toxicity of lead means that there is interest in finding a nontoxic substitute. Bulk single crystals of both cubic $CH_3NH_3SnI_3$ and $CH(NH_2)_2SnI_3$ were obtained by using the top-seeded solution growth method under an ambient atmosphere. Structural refinement, band gap, thermal properties, and XPS measurements of $CH_3NH_3SnI_3$ and $CH(NH_2)_2SnI_3$ single crystals are also reported in detail. These results should pave the way for further applications of $CH_3NH_3SnI_3$ and $CH(NH_2)_2SnI_3$.*

Lead-containing organic–inorganic hybrid perovskite materials are of great interest for photovoltaic applications.[1] Increases in power conversion efficiencies (PCEs) from 3.8%[2] to 20.1%[3] have been reported over the past six years. Since the toxicity of lead is of concern, a nontoxic substitute for perovskite materials is required. The Pb could be replaced with Sn or Ge, which are in the same group in the periodic table. However, the stability of the 2+ oxidation state decreases on descending the group, so these materials may not be stable.[4]

Recent reports[4–8] on $CH_3NH_3SnI_3$ ($MASnI_3$) and $CH(NH_2)_2SnI_3$ ($FASnI_3$) materials mainly focus on hybrid tin halide perovskite polycrystalline and thin films. To the best of our knowledge, there are few previous reports on solar cells using Sn-based perovskite materials as the absorber layer, although PCEs from about 6% to 8.5% have been reported by Kanatzidis,[5,6,15] Snaith,[4] and their respective co-workers. On the other hand, single crystals are important for studies of the basic properties of materials in the absence of grain boundary effects. There have been many questions about the lower PCEs and stability of tin iodide perovskite materials. Most of the previous reports on the properties of $MASnI_3$ and $FASnI_3$ used single crystals that were synthesized and grown under inert (Ar or N_2) atmospheres.[7–14] There were no reports on the growth of bulk $MASnI_3$ and $FASnI_3$ single crystals under an ambient atmosphere, because of the instability of these materials. We have obtained both cubic $MASnI_3$ and $FASnI_3$ single crystals with dimensions of 20 mm × 16 mm × 10 mm and 8 mm × 6 mm × 5 mm (Figure 1) under an ambient atmosphere by using the top-seeded solution growth (TSSG) method. Detailed structural refinements and measurements of the band gap and thermal properties of $MASnI_3$ single crystals have also been carried out. The bandgaps of $MASnI_3$ and $FASnI_3$ single crystals are approximately 1.15 eV and 1.4 eV, respectively. The crystals exhibit relatively good physical and chemical stability when exposed to inert atmospheres. The thermal expansion coefficients α_{11} of $MASnI_3$ and $FASnI_3$ along all the axial directions were calculated to be $3.423 \times 10^{-5}\ K^{-1}$ and $3.667 \times 10^{-5}\ K^{-1}$, respectively. These properties of $MASnI_3$ and $FASnI_3$ single crystals pave the way for further applications in optoelectronics.

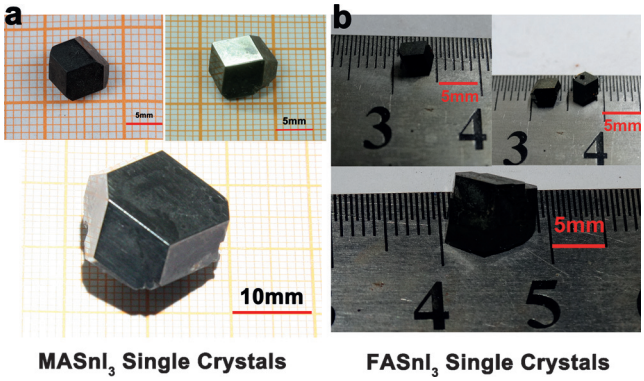

Figure 1. a) $MASnI_3$ and b) $FASnI_3$ single crystals obtained by optimizing crystal growth conditions. Scale bars in the upper images in (a): 5 mm.

In the synthesis, formamidinium acetate or freshly synthesized MAI was reacted with SnO in a mixed solution of HI–H_3PO_2 at 75 °C under air. Seed crystals were obtained by spontaneous crystallization. The crystal growth conditions were optimized by using growth temperature control and high-quality seed-crystal selection. Phase purity was observed, and no impurities were found. The powder XRD diffraction patterns were both in good agreement with the calculated XRD diffraction patterns of the single crystals in Figure 2.

The solubility curves of $MASnI_3$ and $FASnI_3$ in an HI–H_3PO_2 mixed solution are shown in Figure 3; these solubility data are needed to ensure good crystal growth. The solubility of $MASnI_3$ becomes higher than that of $FASnI_3$ as the temperature is increased. $MASnI_3$ was saturated at 65 °C, while $FASnI_3$ was saturated at 60 °C. The H_3PO_2 solution was used as a reducing regent to stabilize the Sn^{2+} and I^- ions in $MASnI_3$ and $FASnI_3$ during the crystal growth. This proce-

[*] Y. Dang, Y. Zhou, X. Liu, D. Ju, Prof. Dr. S. Xia, Prof. Dr. H. Xia, Prof. Dr. X. Tao
State Key Laboratory of Crystal Materials, Shandong University
No. 27 Shanda South Road, Jinan, 250100 (P.R. China)
E-mail: txt@sdu.edu.cn

Supporting information for this article can be found under http://dx.doi.org/10.1002/anie.201511792.

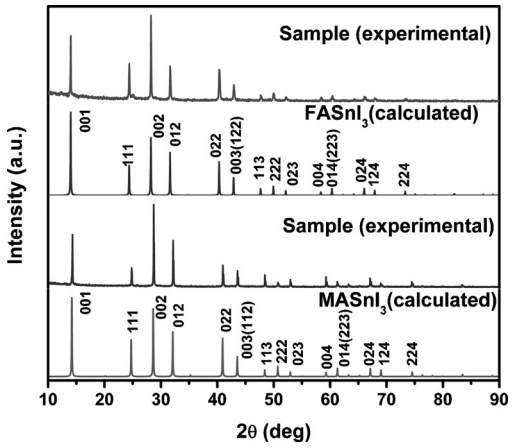

Figure 2. Experimental and calculated powder X-ray diffraction patterns for $MASnI_3$ and $FASnI_3$. The powder XRD patterns of the samples were in consistent with the calculated XRD patterns of $MASnI_3$ and $FASnI_3$ single crystals.

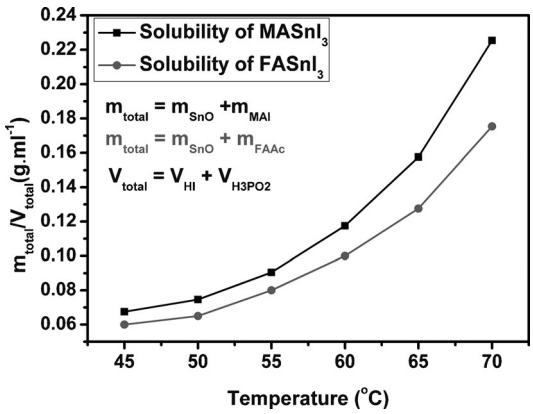

Figure 3. Solubility curves of $MASnI_3$ and $FASnI_3$ in an $HI–H_3PO_2$ mixed solution. The data shows the solubility of $MASnI_3$ (squares) and $FASnI_3$ (circles) at different temperatures to ensure the crystal growth.

dure ensured that no byproducts were obtained because of the presence of H_3PO_2/H_3PO_3 redox potentials in the reaction.

X-ray diffraction studies indicate that the crystal structures of $MASnI_3$ and $FASnI_3$ both belong to the cubic $Pm\bar{3}m$ (no. 221) space group at room temperature. The related single-crystal parameters are presented in Tables S1–S7 (see the Supporting Information). The related lattice parameters for $FASnI_3$ are all larger than those for $MASnI_3$, which agree with those previously reported.[8] As already described,[7] $MASnI_3$ exhibited a distorted noncentrosymmetric tetragonal $P4mm$ (no. 99) three-dimensional perovskite structure at room temperature, while the crystal structures of $FASnI_3$ belonged to $Amm2$ (no. 38) and $Imm2$ (no. 44) space groups, at 340 K and 180 K, respectively. However, we redetermined and refined the crystal structure of $MASnI_3$ and $FASnI_3$, and the results indicated that they both belonged to the cubic system, similar to those of previously reported.[8–14] Ball-and-stick diagrams of the crystal structure are shown in Figure 4. C and N atoms in the C/N structural

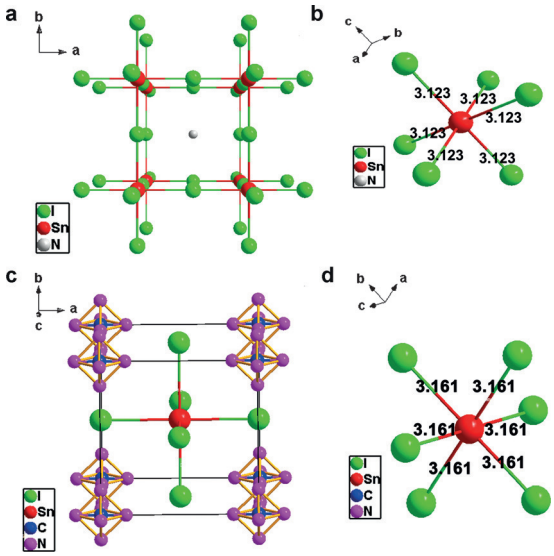

Figure 4. Ball-and-stick stick diagrams of crystal structures and the $\{SnI_6\}$ octahedral structure units in the $MASnI_3$ and $FASnI_3$ single crystals. Along the [001] direction, the crystal structure of $MASnI_3$ (a) and $FASnI_3$ (c); the C and N elements represent the disordered CH_3NH_3 and $CH(NH_2)_2$ groups; hydrogen atoms bonded to the C or N atoms were omitted for clarity. In the $\{SnI_6\}$ octahedral structure unit of $MASnI_3$ (b) and $FASnI_3$ (d), all the I–Sn bond lengths were 3.123 Å and 3.161 Å, respectively.

unit of $MASnI_3$ and $FASnI_3$ exist in the presence of disorder phenomena so that the distribution of C and N atoms was random around the C–N bond. All of the I–Sn bond lengths in the structure of $FASnI_3$ were found to be 3.161 Å, which were longer than those of $MASnI_3$ (3.123 Å), thus indicating the symmetry of the $\{SnI_6\}$ octahedral structural unit along the different directions.

The UV/Vis/NIR diffuse reflectance spectra for $MASnI_3$ and $FASnI_3$ are given in Figure S1. Calculations of the band structure indicate that $MASnI_3$ and $FASnI_3$ are bandgap materials by a narrow margin.[7,8,13] Hall effect measurements at room temperature show that $MASnI_3$ single crystals show p-type semiconductor behavior, while $FASnI_3$ single crystals show n-type semiconductor behavior, which is consistent with previous reports.[7] Their trap densities (carrier concentration) were both in the order of 10^{11} cm^{-3} (see Figure S5). The bandgap can be determined from where a tangent to the $F(R)$–energy curve intersects the x-axis. The absorption spectrum was calculated from the reflectance spectrum by using the Kubelka–Munk function $F(R) = \alpha/S = (1-R)^2/(2R)$, where α is the absorption coefficient, S is the scattering coefficient, and R is the reflectance.[17] The UV/Vis/NIR spectrum for $MASnI_3$ (Figure S1 a) immediately after crystal growth indicates that the band gap of $MASnI_3$ is approximately 1.15 eV, which is smaller than reported for polycrystals[7] and thin films.[4–6] However, after exposure to an ambient atmosphere for one month, the UV/Vis/NIR spectrum of $MASnI_3$ (Figure S1 b) indicates that the bandgap has increased to 1.46 eV. The blue-shift of the absorption peak in the UV/Vis/NIR spectrum is attributed to oxidation of Sn^{2+} into Sn^{4+}. The powder XRD patterns and photograph of

$MASnI_3$ (Figure S2a and S2c) clearly verified the phenomena. Although the UV/Vis/NIR spectrum of $FASnI_3$ (Figure S1c) implies that the bandgap of $FASnI_3$ is approximately 1.4 eV (which is higher than that of $MASnI_3$) both immediately after crystal growth and after exposure to an ambient atmosphere, while there is no change in the powder XRD patterns (Figure S2d). Furthermore, XPS measurements were used to characterize the oxidation state of Sn in the $MASnI_3$ and $FASnI_3$ single crystals immediately after crystal growth and after exposure to an ambient atmosphere for one month. The Sn 3d5 peak at binding energies from 490 to 484 eV shows the oxidation state of Sn (Figure S4). The main band at around 487 eV can be attributed to Sn^{2+}.[18] The oxidation state of Sn in $FASnI_3$ after one month under an ambient atmosphere remains unchanged. However, exposure of $MASnI_3$ to an ambient atmosphere for one month results in the formation of Sn^{2+} and Sn^{4+}, which explains the additional peak at about 488 eV (Figure S4c) that can be attributed to the presence of Sn^{4+}, and is in agreement with previous observations.[18] This result is consistent with the changes of band gap and powder XRD patterns of $MASnI_3$ (Figure S1b and S2c, respectively). These behaviors show that $FASnI_3$ is more stable than $MASnI_3$ upon exposure to the ambient atmosphere.

The thermal expansion coefficients and the specific heat values of $MASnI_3$ and $FASnI_3$ single crystals were measured. Figure 5a and 5b show the measured thermal expansion along the [100] direction. The change of thickness ΔL increases almost linearly with temperature. The thermal expansion coefficients have been calculated using Equation (1):

$$\alpha(T - T_0) = \frac{1}{\Delta T}\frac{\Delta L}{L} \tag{1}$$

For the cubic crystal with space group of $Pm\bar{3}m$, there is only one independent thermal expansion coefficient α_{11} [Equation (2)]. The thermal expansion coefficients of $MASnI_3$ and $FASnI_3$ are calculated to be $3.423 \times 10^{-5}\ K^{-1}$ and $3.667 \times 10^{-5}\ K^{-1}$, respectively.

$$\begin{pmatrix} a_{11} & 0 & 0 \\ 0 & a_{11} & 0 \\ 0 & 0 & a_{11} \end{pmatrix} \tag{2}$$

The specific heat (C_p) value of $MASnI_3$ or $FASnI_3$ as a function of temperature is shown in Figure 5c and 5d. These values of $MASnI_3$ and $FASnI_3$ both increase almost linearly with increasing temperature from $0.805\ J\,(g\,K)^{-1}$ at 296 K to $0.97\ J\,(g\,K)^{-1}$ at 420 K and from $0.357\ J\,(g\,K)^{-1}$ at 296 K to $0.42\ J\,(g\,K)^{-1}$ at 390 K, respectively.

The decomposition temperature of $MASnI_3$ single crystals is 200 °C, which is higher than that of $FASnI_3$ (175 °C), thus indicating that they both have relatively good thermal stability (Figure 6). $MASnI_3$ starts to lose weight under 200 °C, while $FASnI_3$ begins to lose weight under 175 °C. These results indicate that the residues are both mainly SnI_2, which are consistent with the with mass loss of the organic cations and the tin iodide residues reported by Kanatzidis an co-workers.[7] The reactions that occur under a flow of N_2 gas are given in Equations (3) and (4):

$$MASnI_3\,(s) = FAI\,(g) + SnI_2\,(s); \tag{3}$$

$$FASnI_3\,(s) = MAI\,(g) + SnI_2\,(s). \tag{4}$$

Although they are both hygroscopic and air-sensitive when exposed to the ambient atmosphere, the black $MASnI_3$ and $FASnI_3$ single crystals were stable under an inert (Ar or N_2) atmosphere for several months, as shown by powder XRD measurements (Figure S3). In particular, the stability of $FASnI_3$ is better than that of $MASnI_3$ after exposure to the ambient atmosphere for one month (Figure S2).

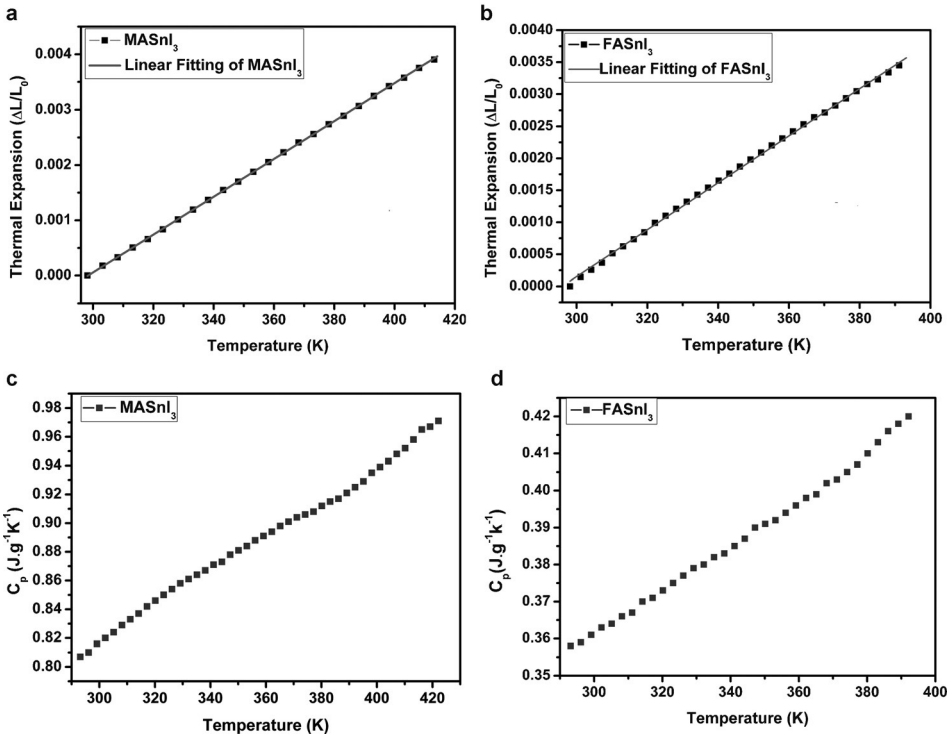

Figure 5. Thermal expansion and specific heat capacities of $MASnI_3$ and $FASnI_3$ single crystals along the [100] direction. a) Thermal expansion of $MASnI_3$ measured in the temperature range 296–420 K and (c) specific heat capacity measurement of $MASnI_3$ performed under a nitrogen atmosphere in the temperature range 296–420 K. b) Thermal expansion of $FASnI_3$ conducted in the temperature range 296–400 K and d) specific heat capacity measurement of $FASnI_3$ performed under a nitrogen atmosphere in the temperature range 296–390 K.

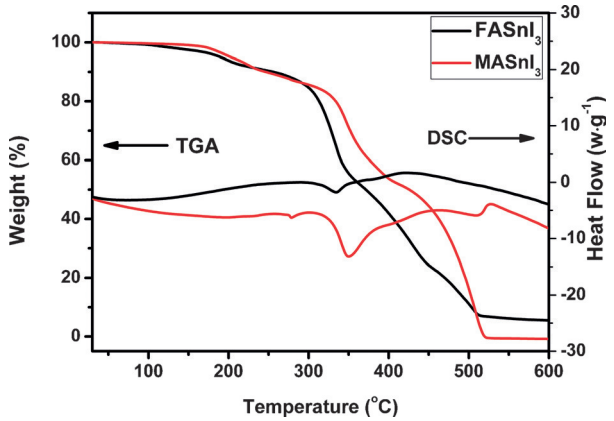

Figure 6. TGA and DSC data for $MASnI_3$ (red line) and $FASnI_3$ (black line).

In summary, we have investigated bulk $MASnI_3$ and $FASnI_3$ single crystals by using a TSSG method under an ambient atmosphere. Detailed measurements such as structural refinement, bandgap, thermal properties, and XPS have been also conducted. $MASnI_3$ single crystals are p-type semiconductors, while $FASnI_3$ single crystals are n-type semiconductors. The trap densities in these crystals are in the order of 10^{11} cm^{-3}. Although they are air-sensitive, both $MASnI_3$ and $FASnI_3$ single crystals are stable under inert atmospheres. In particular, the stability of $FASnI_3$ is higher than that of $MASnI_3$. Our studies provide new information about the fundamental properties of $MASnI_3$ and $FASnI_3$ single crystals, and potentially provide guidance for the applications in solar cells, field-effect transistors (FETs), and thermoelectric devices. Further studies on the other properties of $MASnI_3$ and $FASnI_3$ single crystals are underway.

Experimental Section

Reagents: Analytical-grade reactants of SnO, formamidinium acetate ($NH{=}CHNH_2CH_3OOH$), CH_3NH_2 (H_2O) solution, H_3PO_2 solution and HI solution were purchased from Sinopharm Co. Ltd. and used without further purification.

Synthesis and crystal growth: Synthesis and crystal growth were conducted based on a previously reported procedure.[16]

Synthesis of $MASnI_3$: The raw materials were dissolved at 75 °C under an ambient atmosphere. SnO (20.210 g, 0.15 mol) and freshly synthesized MAI (23.850 g, 0.15 mol) were dissolved in a mixture of HI (150 mL) and H_3PO_2 (150 mL) and were stirred to form a bright-yellow solution. The solutions were saturated at 65 °C. A black, shiny single crystal of $MASnI_3$ was grown in about one month by top-seeded solution growth.

Synthesis of $FASnI_3$: SnO (13.471 g, 0.10 mol) and formamidinium acetate (10.411 g, 0.10 mol) were dissolved in a mixture of HI (135 mL) and H_3PO_2 (135 mL) solution and were stirred to form a bright-green solution. Solutions were saturated at 60 °C. A black, shiny $FASnI_3$ single crystal was grown in about one month by top-seeded solution growth (Figure 1).

Characterization: Methods for XRD, structural refinement, bandgap, thermal properties, XPS, and Hall Effect measurements are given in the Supporting Information. CCDC 1429424, 1438332, for $MASnI_3$ and $FASnI_3$ contain the supplementary crystallographic data for this paper. These data can be obtained free of charge from The Cambridge Crystallographic Data Centre.

Acknowledgements

We greatly appreciate the help of Prof. Dr. Kenneth A. Jackson (member of the National Academy of Engineering), University of Arizona, Tucson, in modifying the manuscript. This work was supported by the National Natural Science Foundation of China (grant nos. 51321091, 51227002, 51272129) and the Program of Introducing Talents of Disciplines to Universities in China (111 program no. b06015). We greatly thank Qingming Lu, Zhongjun Zhai, Xiufeng Cheng, and Xiulan Duan for their help in crystal orientation, crystal processing, thermal properties and XPS measurements, respectively.

Keywords: band gaps · crystal growth · perovskites · semiconductors · tin

How to cite: *Angew. Chem. Int. Ed.* **2016**, *55*, 3447–3450
Angew. Chem. **2016**, *128*, 3508–3511

[1] J. Shi, X. Xu, D. Li, Q. Meng, *Small* **2015**, *11*, 2472–2486.
[2] A. Kojima, K. Teshima, Y. Shirai, T. Miyasaka, *J. Am. Chem. Soc.* **2009**, *131*, 6050–6051.
[3] W. S. Yang, J. H. Noh, N. J. Jeon, Y. C. Kim, S. Ryu, J. Seo, S. I. Seok, *Science* **2015**, *348*, 1234–1237.
[4] N. K. Noel, S. D. Stranks, A. Abate, C. Wehrenfennig, S. Guarnera, A.-A. Haghighirad, A. Sadhanala, G. E. Eperon, S. K. Pathak, M. B. Johnston, A. Petrozza, L. M. Herz, H. J. Snaith, *Energy Environ. Sci.* **2014**, *7*, 3061–3065.
[5] F. Hao, C. C. Stoumpos, D. H. Cao, R. P. H. Chang, M. G. Kanatzidis, *Nat. Photonics* **2014**, *8*, 489–494.
[6] F. Hao, C. C. Stoumpos, P. Guo, N. Zhou, T. J. Marks, R. P. H. Chang, M. G. Kanatzidis, *J. Am. Chem. Soc.* **2015**, *137*, 11445–11452.
[7] C. C. Stoumpos, C. D. Malliakas, M. G. Kanatzidis, *Inorg. Chem.* **2013**, *52*, 9019–9038.
[8] D. B. Mitzi, K. Liang, *J. Solid State Chem.* **1997**, *134*, 376–381.
[9] D. Weber, *Z. Naturforsch. B* **1978**, *33*, 862–865.
[10] K. Yamada, T. Matsui, T. Tsuritani, T. Okuda, S. Ichiba, *Z. Naturforsch. A* **1990**, *45*, 307–312.
[11] D. B. Mitzi, C. A. Feild, Z. Schlesinger, R. B. Laibowitz, *J. Solid State Chem.* **1995**, *114*, 159–163.
[12] K. Yamada, K. Nakada, Y. Takeuchi, K. Nawa, Y. Yamane, *Bull. Chem. Soc. Jpn.* **2011**, *84*, 926–932.
[13] Y. Takahashi, R. Obara, Z.-Z. Lin, Y. Takahashi, T. Naito, T. Inabe, S. Ishibashi, K. Terakura, *Dalton Trans.* **2011**, *40*, 5563–5568.
[14] Y. Takahashi, H. Hasegawa, Y. Takahashi, T. Inabe, *J. Solid State Chem.* **2013**, *205*, 39–43.
[15] I. Chung, B. Lee, J. He, R. P. H. Chang, M. G. Kanatzidis, *Nature* **2012**, *485*, 486–489.
[16] Y. Dang, Y. Liu, Y. Sun, D. Yuan, X. Liu, W. Lu, G. Liu, H. Xia, X. Tao, *CrystEngComm* **2015**, *17*, 665–670.
[17] W. M. Wendlandt, H. G. Hecht, *Reflectance Spectroscopy*, Interscience, New York, **1966**, p. 62.
[18] M. Weiss, J. Horn, C. Richter, D. Schlettwein, *Phys. Status Solidi A* **2015**, DOI: 10.1002/pssa.201532594.

Received: December 21, 2015

